• Basic Research •

Cuproptosis-related signature and immune infiltration in age-related macular degeneration

Chen Li[1], *Yi-Cheng Lu*[1], *Ming-Xuan Chen*[2]

[1]Department of Ophthalmology, the First Affiliated Hospital of Soochow University, Suzhou 215006, Jiangsu Province, China
[2]School of Clinical Medicine, Medical College of Soochow University, Suzhou 215006, Jiangsu Province, China
Correspondence to: Chen Li. Department of Ophthalmology, the First Affiliated Hospital of Soochow University, Suzhou 215006, Jiangsu Province, China. lceye0902@126.com
Received: 2024-07-15 Accepted: 2025-05-21

Abstract

● **AIM:** To investigate cuproptosis-related molecular and immune infiltration in age-related macular degeneration (AMD) development and establish a predictive model.

● **METHODS:** The expression profiles of cuproptosis-related genes and immune signature in AMD based on the microarray dataset GSE29801 were analyzed. A total of 142 AMD samples were used to identify the cuproptosis-related differentially expressed genes (Cu-DEGs), together with the immune cell infiltration. To further refine the list of potential genes for AMD diagnosis, three machine learning techniques were used, and an external dataset were applied for confirming the accuracy of the predictive performance. Reverse transcription polymerase chain reaction (RT-PCR) were also performed to examine the level of mRNA of hub genes. The activated immune responses and Cu-DEGs were assessed between AMD and controls.

● **RESULTS:** Six genes, including *ATP7A*, *DBT*, *VEGFA*, *UBE2D3*, *CP*, *SLC31A1*, were screened as cuproptosis-signature in AMD *via* three machine learning methods. Next, *SLC31A1* and *VEGFA* was selected as hub genes by performance evaluation in an external dataset GSE160011, further analysis showed that *SLC31A1* and *VEGFA* were associated with pathways related to immune signaling and immune function, which were then observed in relation to infiltrating immune cells. Finally, the mRNA expression levels of *SLC31A1* and *VEGFA* were significantly higher in laser induced choroidal neovascularization (CNV) group than in control group detected by RT-PCR.

● **CONCLUSION:** In this study, the possible relationship between cuproptosis and AMD is expounded systematically. A predictive model is developed to assess the risk of cuproptosis-related genes and their clinical prognostic value in AMD patients.

● **KEYWORDS:** age-related macular degeneration; cuproptosis; immune infiltration; machine learning
DOI:10.18240/ijo.2025.09.04

Citation: Li C, Lu YC, Chen MX. Cuproptosis-related signature and immune infiltration in age-related macular degeneration. *Int J Ophthalmol* 2025;18(9):1640-1649

INTRODUCTION

Age-related macular degeneration (AMD) is a serious visual impairment, which is the primary cause of irreversible blindness in the elderly population worldwide[1]. AMD is divided into two types: wet AMD and dry AMD. Wet AMD, also known as neovascular AMD (nAMD), is primarily caused by compromised permeability of the blood-retina barrier and abnormal retinal blood supply. Choroidal neovascularization (CNV) is the key feature of nAMD, in which abnormal proliferation of choroidal neovascularization, result in intra- and sub-retinal macular edema, fluid accumulation, hemorrhage, and retinal tissue destruction. Anti-VEGF treatment is widely used in clinical practice, but not all patients benefit from it equally. Dry AMD usually involves at first retinal pigment epithelial (RPE) cells, which in turn promotes photoreceptor cells damage, for which there remains to be a lack of effective treatments at present[2]. AMD does not have very apparent symptoms, especially in the early stage, and early diagnosis is difficult. It is often too late to rescue by the time a patient visits an ophthalmologist as the treatment cannot regenerate the vision. Therefore, it is of huge significance to identify the specific molecular mechanism of the occurrence and development of AMD and to provide effective suggestions to prevent and cure.

Common forms of cell death include apoptosis, pyroptosis, necrosis, and ferroptosis. Recently, cuproptosis, a unique copper-induced cell death mediated by ionophores, has been identified with significant pathophysiological roles. Excessive copper enters mitochondria-dependent cells *via* ionophores and binds to dihydrolipoamide acetyltransferase, triggering its heterodimerization and insoluble aggregate formation,

Table 1 Details in GSE29801

Diagnosis	GSM738433-GSM738607 (RPE-choroid samples from macular or extramacular region)	GSM738608-GSM738725 (retinal samples from macular or extramacular region)
Normal	96	55
AMD	79	63
Dry AMD	30	30
MD1	11	9
MD2	8	5
CNV	8	9
GA	4	4
GA/CNV	6	6
Clinical AMD diagnosis	12	0

Normal: No signs of ocular abnormalities; AMD: Age-related macular degeneration; Dry AMD: Soft indistinct or reticular drusen only, soft distinct drusen with pigmentary abnormalities, or soft indistinct or reticular drusen with pigmentary abnormalities; MD1: Hard macular drusen only; MD2: Soft distinct drusen only; CNV: Sub-retinal choroidal neovascularization; GA: Sharply demarcated area of apparent absence of the RPE (>175 μm) involving central macular region; GA/CNV: Geographic atrophy with choroidal neovascularization. GSE: Gene series; GSM: Gene sample; RPE: Retinal pigment epithelium; AMD: Age-related macular degeneration; MD1: Pre-AMD; MD2: Sub-clinical pre-AMD; CNV: Choroidal neovascularization; GA: Geographic atrophy.

ultimately leading to cytotoxicity. Dysregulated copper homeostasis, primarily regulated by mitochondrial function, can also induce cell death[3]. Cuproptosis contributes to ocular diseases; for instance, the cuproptosis-related gene *SLC31A1* serves as a diagnostic biomarker for diabetic retinopathy and may mediate cuproptosis in retinal microglia[4]. In AMD, reactive oxygen species accumulation in RPE causes mitochondrial dysfunction, forcing energy reliance on glycolysis and resulting in photoreceptor degeneration[5]. Mitochondrial dysfunction-induced metabolic insufficiency and oxidative stress are key AMD mechanisms. Reduced copper levels and downregulated SLC31A1 in AMD patients' RPE/choroid, alongside clinical evidence linking higher copper intake to lower nAMD risk, suggest copper's involvement in nAMD pathogenesis[6-8]. Cuproptosis is characterized by copper binding to lipoylated tricarboxylic cycle components, while elevated tricarboxylic substrates in nAMD patients imply its potential role in AMD progression[3,9].

To explore the possible pathogenesis of cuproptosis in AMD, we downloaded chip data from the Gene Expression Omnibus (GEO) database for AMD samples and control samples. Then, the intersect genes of cuproptosis-related genes were extracted to identify the cuproptosis-related differentially expressed genes (Cu-DEGs). We performed immune infiltration analysis and analyzed the correlation between Cu-DEGs and immune cells subsequently. In order to find the characteristic genes associated with cuproptosis in AMD and identify candidate biomarkers, we construct and validate prognostic gene signatures for AMD *via* Least absolute shrinkage and selection operator (Lasso) regression, Support vector machine (SVM) algorithms and Random Forest algorithms three methods and further explore their clinical diagnostic value.

In this study, we explored the potential molecular mechanism related to cuproptosis in AMD from multiple perspectives for the first time, and screened out biomarkers with clinical diagnostic value, providing a new molecular theoretical basis for the treatment of AMD. In addition, we verified the expression levels of two biomarkers *in vitro* experiment.

MATERIALS AND METHODS

Ethical Approval Data were obtained from the GEO database, which houses ethically approved, publicly available datasets. Our bioinformatics analysis used anonymized data, thus exempting this study from additional ethical review. Animal experiments were approved by the Animal Ethics Committee of Soochow University (No.SUDA202205A0251) and complied with institutional guidelines.

Data Acquisition and Pre-processing Microarray datasets (GSE29801, GSE160011) related to AMD were obtained from the GEO (http://www.ncbi.nlm.nih.gov/geo/). The GSE29801 dataset (GPL4133 platform) included RPE-choroid and retina tissues from 26 AMD (33 males and 46 females, age range 43-101y), 11 potential pre-AMD, and 31 normal controls (58 males and 38 females, age range 9-93y). It contained 151 normal samples (96 RPE-choroid samples: 58 males/38 females; 55 retinal samples: 30 males/25 females) and 142 AMD samples (79 RPE-choroid samples: 33 males/46 females; 63 retinal samples: 27 males/36 females)[10]. Details are provided in Table 1. The GSE160011 dataset (GPL19057 platform) was selected for validation analysis, which included retina microglia tissues from 6 laser induced CNV samples and 6 un-lasered controls[11]. Raw data was log2 transformed prior to analysis. Microarrays were further processed using "limma" R package[12].

Identification of the Cu-DEGs The cuproptosis-related genes were compiled from the Molecular Signature Database

(MsigDB, http://www.gsea-msigdb.org/gsea/msigdb/) and the published studies[13-16]. After we got rid of the duplicates, we found 41 common genes that are involved in cuproptosis. After that, differentially expression analysis (Cutoff: $P<0.05$ and $\log_2|\text{fold change}|\geq 1$) was used to identify the Cu-DEGs.

Evaluating the Immune Cell Infiltration The CIBERSORT method with LM22 signature matrix were applied from CIBERSORT online tool (https:/cibersort.stanford.edu/) to quantify the sample's immune cell infiltration levels. CIBERSORT, using Monte Carlo sampling, derives an empirical *P*-value for each sample. Only samples with $P<0.05$ were deemed to be accurate immune cell fractions[17].

Correlation Analysis Between Cu-DEGs and Infiltrated Immune Cells To determine correlation between Cu-DEGs and AMD-related immune cell properties, correlation coefficients were calculated between the Cu-DEGs expression and the relative percentage of immune cells. Significance for spearman correlation coefficients was set at $P<0.05$. Eventually, the presentation of results was performed using the "corrplot" R package (http://github.com/taiyun/corrplot).

Machine Learning Three machine learning methods were applied to further filter the list of potential genes for AMD diagnosis. Lasso is a data mining method based on multiple linear regression. By adding penalty coefficient and continuously compressing coefficient, the model can be simplified, and variables can be filtered. It can make use of a small sample for efficient screening[18]. SVM is a supervised machine learning algorithm based on statistical learning theory. It minimizes the actual risk by seeking to reduce the result risk. It can solve nonlinear data well and is suitable for small sample prediction[19]. Random Forest is also a supervised algorithm that uses many decision trees to form an integrated method that can be used for classification or regression[20]. The Lasso regression, SVM, and Random Forest analyses were performed using the R packages "glmnet" (https://www.jstatsoft.org/v33/i01/), "kernlab" (https://doi.org/10.18637/jss.v011.i09) and "randomForest" (https://CRAN.R-project.org/doc/Rnews/). The intersection genes of them were considered as cuproptosis signature in AMD diagnosis.

Performance Evaluation of Hub Genes in External Data Set The expression of hub genes was verified in GSE160011. The GSE160011 dataset contains retina microglia tissues from 6 laser induced CNV samples and 6 un-lasered controls. The comparison between the two sets of data was performed with the *t*-test. $P<0.05$ was considered significant. Receiver operating characteristic (ROC) analysis was performed with "pROC" package (http://www.biomedcentral.com/1471-2105/12/77/).

Gene Set Enrichment Analysis Gene set enrichment analysis (GSEA) was employed to detect the biological signaling pathways in hub genes, which was performed using the R package "clusterProfiler"[21]. The enrichment results were displayed based on net enrichment score, gene ratio, and *P* value. |Net enrichment score|>1 and false discovery rate (FDR) $Q<0.25$ were considered to represent significant enrichment.

Laser-induced CNV Model We employed laser induced CNV mice, a commonly used model of nAMD. C57 mice were anesthetized with Avertin anesthetic (0.15 mL/10 g) by intraperitoneal injection and dilated with compound tropicamide eye drops (Santen, Japan). To prevent corneal matrix opacity, ophthalmic gel was applied to maintain corneal moist during the laser process. After pupil dilation, mice were placed in front of Nd:YAG laser (VISULAS Trion, Zeiss, Germany). The laser wavelength was 532 nm, the energy was 240 mA, and the spot size was 50 μm. The right eye of each mouse was selected for experiment. Laser was irradiated on the macula to induce CNV (4 sites per eye, 6 eyes per group). Formation of a bubble at the time of laser application indicates rupture of Bruch membrane, which is an important factor for successful induction of CNV. Five days after the modeling, fundus fluorescein angiography observed macular exudation, indicating successful modeling. After successful modeling, choroid tissues were taken one day, five days after modeling and placed in TRIzol solution for further analysis.

Reverse Transcription Polymerase Chain Reaction Validation To verify the mRNA expression of the hub genes *SLC31A1* and *VEGFA*, Reverse transcription polymerase chain reaction (RT-PCR) was performed using a RT-PCR kit (Takara bio, Japan). In simple terms, total RNA was isolated using TRIzol, followed by reverse transcription of RNA into cDNA using random primers and Oligo (dT), followed by qPCR using a three-step method. The relative quantification of lncRNA was calculated by $2^{-\Delta\Delta Ct}$ method, and GAPDH was used as reference after normalization. The RT-PCR template sequence was *SLC31A1*: forward: 5'-TATGGGTATGTACCACACGGAC-3'; reverse: 5'-GCCATTTCTCCAGGTGTATTGA-3'; *VEGFA*: forward: 5'-AGGGCAGAATCATCACGAAGT-3'; reverse: 5'-GCCATTTCTCCAGGTGTATTGA-3'; *GAPDH*: forward: 5'-CATGGCCTTCCGTGTTCCTA-3'; reverse: 5'-CGCCTCCTTTTCCTCTCAT-3'.

Software and Versions R Studio (Version 4.2.2) was used for statistical analysis and graphs.

RESULTS

Identification of the Cu-DEGs in AMD The process of our study was shown in the flowchart in Figure 1. By downloading and overlapping cuproptosis datasets with microarray datasets GSE 29801, 41 common genes were obtained by intersection of the Venn diagram (Figure 2A). A total of 10 Cu-DEGs were obtained through analysis ($P<0.05$ and $\log_2|\text{fold change}|\geq 1$), and volcano plots were displayed (Figure 2B). Afterwards,

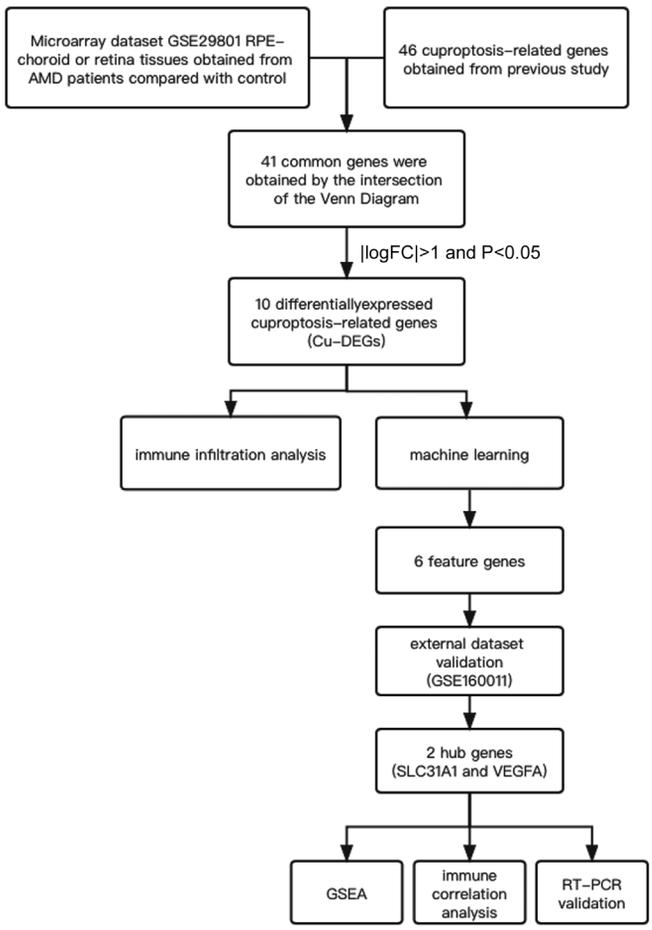

Figure 1 Flow chart showing the research process in this study RPE: Retina pigment epithelium; AMD: Age-related macular degeneration; DEGs: Differential expressed genes; Cu-DEGs: Cuproptosis-related DEGs; GSEA: Gene set enrichment analysis; GSE: Gene series; RT-PCR: Reverse transcription polymerase chain reaction.

we performed the correlation analysis between these Cu-DEGs. Among them, *PDK1* and *ULK2*, *PDK1* and *MAP2K1*, *MAP2K1* and *SLC31A1*, *SLC31A1* and *UBE2D3* presented a strong synergistic relationship, while some genes presented a strong antagonistic relationship, such as *PDK1* and *UBE2D3*, *ULK2* and *SLC31A1*, *ULK2* and *UBE2D3* (Figure 2C).

Evaluation of Immune Cell Infiltration To explore whether there were differences in the immune cell role between the AMD and controls, we conducted the immune cell infiltration analysis to shed further light on the immunoregulation of AMD based on the CIBERSORT algorithm. The box plot displayed that AMD patients had a higher proportion of $CD8^+$ T cells, resting memory $CD4^+$ T cells, activated memory $CD4^+$ T cells, activated natural killer (NK) cells, monocytes, M1 macrophages (Figure 3A-3B), suggesting that the alternations in the immune system play a crucial role for the occurrence of AMD. Meanwhile, correlation analysis results indicated that activated mast cells, eosinophils, regulator T cells, neutrophils, naïve B cells, resting NK cells were correlated with Cu-DEGs (Figure 3C). These results suggested that Cu-DEGs may be the critical factors involved in regulating the molecular and immune infiltration status of AMD patients.

Identification of the Cuproptosis Signature *via* Machine Learning To identify cuproptosis signature in AMD, 3 machine-learning algorithms were employed, including Lasso (Figure 4A-4B), SVM (Figure 4C-4D), and Random Forest (Figure 4E-4F). Finally, 6 cuproptosis signatures genes were determined, including *ATP7A*, *DBT*, *VEGFA*, UBE2*D3*, *CP*, *SLC31A1* (Figure 4G).

Validation of Hub Genes Expression In order to verify the reliability of these cuproptosis signature genes expression levels. We selected an external data set containing retina microglia tissues from 6 laser induced CNV samples and 6 un-lasered controls and analyzed the expression levels of 6 cuproptosis signature genes were obtained from previous work. The groups comparison results showed that compared with control, the *SLC31A1* and *VEGFA* expressions were significantly increased in CNV samples (Figure 5A-5B). Among the 6 genes, *SLC31A1* and *VEGFA* had the best predictive accuracy as the area under the curve (AUC) were 0.972 and 0.806, respectively (Figure 5C-5D). Therefore, *SLC31A1* and *VEGFA* were selected as hub genes for further analysis.

GSEA Identifies Hub Genes-Associated Signaling Pathways GSEA was conducted to identify hub genes-related signaling pathways in AMD. Based on "c2.cp.kegg.v7.4.entrez.gmt" as the reference genome, it displayed the top five immune-related gene sets most significantly enriched in *SLC31A1* (Figure 6A) and *VEGFA* (Figure 6B). Gene sets were enriched in the samples of the highly associated *SLC31A1*, including cell adhesion molecules, cytokine-cytokine receptor interaction, extracellular matrix (ECM) receptor interaction, focal adhesion, *etc*. Gene sets were enriched in the samples of the highly associated *VEGFA*, including autoimmune thyroid disease, natural killer cell mediated cytotoxicity, primary immunodeficiency, *etc*. These findings suggest that hub genes were associated with pathways related to immune signaling and function.

Correlation Between Immune Cells and Hub Genes The scatter plot illustrated the relationship between infiltrating immune cells and hub genes. As is shown in the Figure 7, *SLC31A1* was significantly positively correlated to M0 macrophages and naïve B cells, whereas a negative association with M2 macrophages, monocytes, resting mast cells. Positive correlation between *VEGFA* and neutrophils, memory B cells was found, while *VEGFA* negatively correlated with resting mast cells. Besides, the two hub gens showed a strong positive association.

RT-PCR Validation Laser-induced CNV, which is widely used as an animal model for nAMD, reflects at least partially the pathogenesis of human neovascular AMD. To verify the

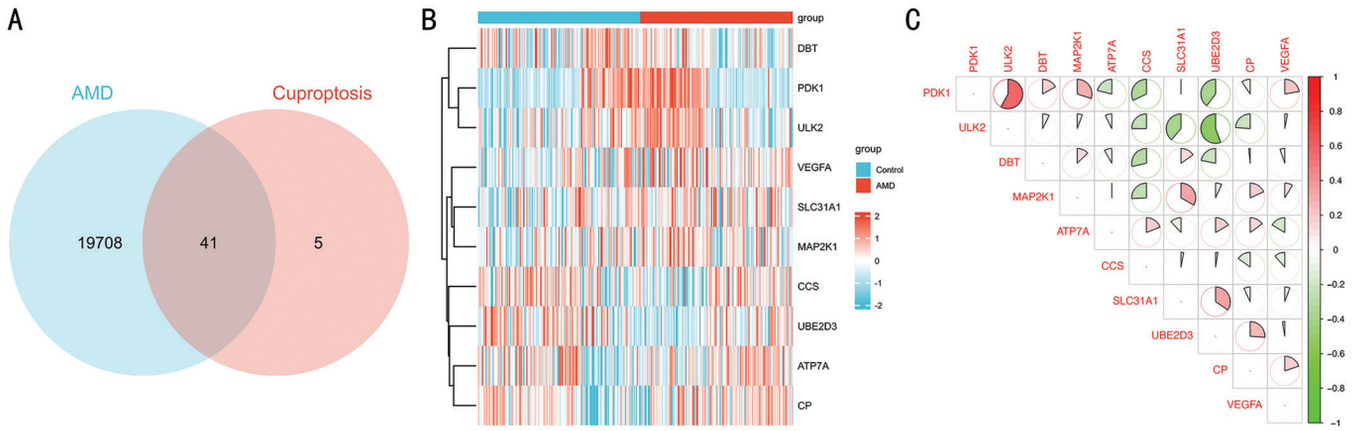

Figure 2 Identification of Cu-DEGs A: Venn plot illustrating the intersection of DEGs from microarray sequencing and cuproptosis-related genes obtained from a previous study. A total of 41 cuproptosis-related genes were identified through this intersection. B: Heatmap showing the expression of 10 Cu-DEGs determined by the screening criteria of $P<0.05$ and $\log_2|\text{fold change}|\geq 1$ in microarray sequencing. Upregulated genes are indicated in red, while downregulated genes are shown in blue. C: Correlation analysis of the 10 Cu-DEGs. The x-axis and diagonal lines represent the Cu-DEGs. The pie charts in the small squares depict the correlation between Cu-DEGs, with red indicating negative correlations and green indicating positive correlations. The area of the pie chart corresponds to the degree of the correlation coefficient; a larger area signifies a more significant correlation between genes. AMD: Age-related macular degeneration; Cu-DEGs: Cuproptosis-related DEGs.

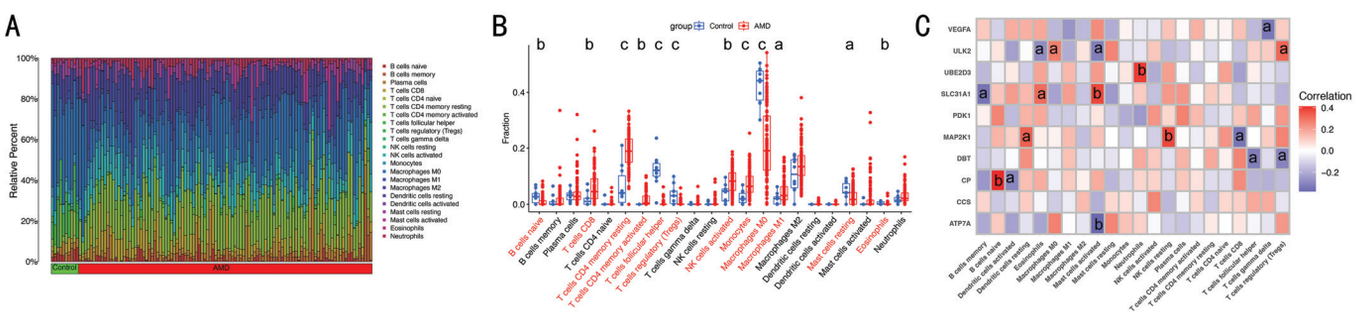

Figure 3 Distribution and visualization of immune cell infiltration A: Histogram illustrating the proportions of 22 immune cell subpopulations in each AMD and control sample. The x-axis represents GEO samples, and the y-axis indicates the percentage of each immune cell type. B: Bar plot showing the differentially infiltrated immune cells between the AMD and control groups. The blue bars represent the AMD group, while the red bars represent the control group. Immune cells with significant differences between the AMD and control groups on the x-axis are marked in red. C: Correlation analysis of immune cells and Cu-DEGs. The numbers in the small squares represent the correlation coefficients between immune cells and Cu-DEGs. The x-axis lists the immune cells, and the y-axis lists the Cu-DEGs. Blue squares indicate a negative correlation, and red squares indicate a positive correlation. [a]$P<0.05$; [b]$P<0.01$; [c]$P<0.001$. AMD: Age-related macular degeneration; GEO: Gene expression omnibus; Cu-DEG: Cuproptosis-related DEGs.

bioinformatics results, RT-PCR experiments were performed. As seen in Figure 8, *SLC31A1* and *VEGFA* mRNA expression levels showed an overall increase in one day and five days after successful modeling versus healthy controls, and the increase of five days was statistically significant ($P<0.01$). This indicates that the bioinformatics results are reliable and have potential research value.

DISCUSSION

Cuproptosis is a novel form of cell death caused by excess copper reported recently. It is mainly mediated by the lipidization of mitochondrial enzymes. When the copper concentration exceeds a certain threshold, it produces lethal effect on cells. Cuproptosis is strongly associated with the progression of various diseases[22-24]. However, cuproptosis and its role in AMD have not been studied. Therefore, we sought to elucidate the specific role of cuproptosis-related genes in AMD phenotypes and immune microenvironments.

The present study analyzed for the first-time comprehensive data on the cuproptosis-related genes expression profile in RPE-choroid or retinal tissues of AMD patients and non-AMD individuals. By differential analysis, we identified 10 Cu-DEGs, indicating that cuproptosis-related genes played an important role in the occurrence of AMD. Subsequently, in order to observe the relationship between cuproptosis-related genes and AMD, we explored the pairwise correlation between 10 Cu-DEGs and found significant synergy or antagonism among these Cu-DEGs. This result confirmed the interaction between Cu-DEGs in AMD. The abundance of immune cells

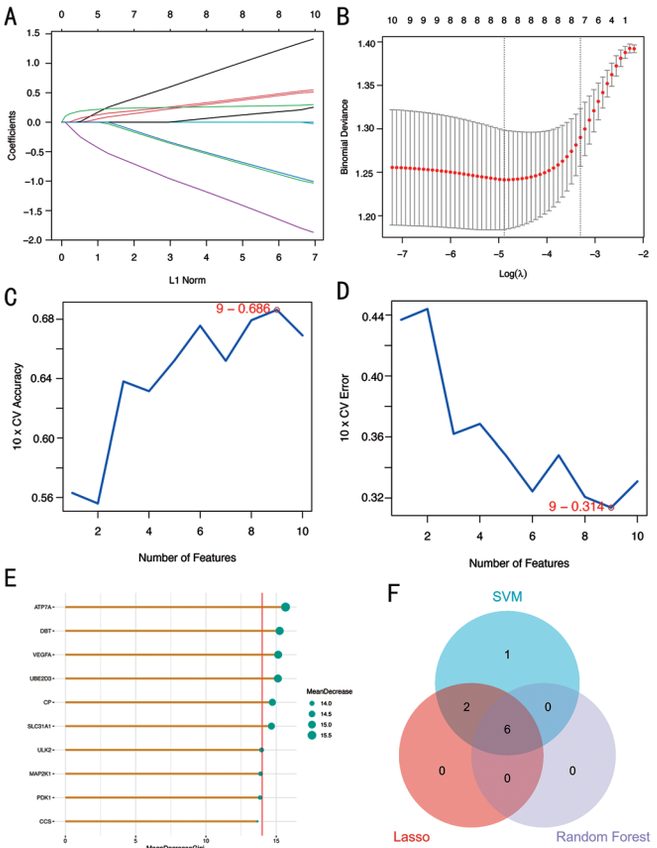

Figure 4 Feature gene selection A, B: Feature selection adjustment using the Lasso model. A: L1 norm of the log(2) transformed gene expression data, illustrating the shrinkage effect of Lasso on different features. B: Cross-validated mean squared error for various values of the regularization parameter (λ), helping to determine the optimal lambda for feature selection. C, D: Biomarker signature gene expression validation using the SVM algorithm. C: Correlation between the number of features and the mean decrease in Gini impurity, indicating the importance of each feature in the classification process. D: Relationship between the number of features and the classification accuracy, demonstrating how the performance changes with the number of selected features. E: Identification of the top six relatively important genes using the Random Forest algorithm. The importance of each gene is measured by the mean decrease in Gini impurity, with higher values indicating greater importance in the classification model. F: Six hub genes were screened by the intersection of the three algorithmic Venn diagrams (Lasso, SVM, and Random Forest). Lasso: Least absolute shrinkage and selection operator; SVM: Support vector machine.

differed significantly between AMD and controls. AMD patients showed higher immune cells infiltration levels, and this result suggested that changes in the immune system may be a key factor in the development of AMD. Through the correlation analysis between Cu-DEGs and immune cells, we found that Cu-DEGs was correlated with mast cells, eosinophils, T cells, neutrophils, B cells and NK cells. Cu-DEGs may be the critical factors involved in regulating the

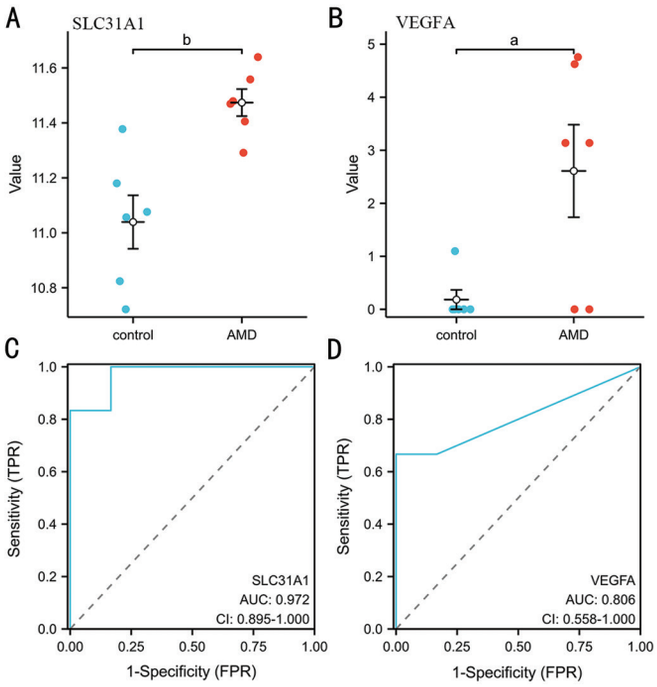

Figure 5 Performance evaluation of hub genes in an external independent GEO dataset GSE160011 A: Box plot showing the expression levels of SLC31A1 in the AMD and control groups. The y-axis represents the expression levels, and the x-axis represents the groups (control and AMD). B: Box plot showing the expression levels of VEGFA in the AMD and control groups. The y-axis represents the expression levels, and the x-axis represents the groups (control and AMD). C: ROC curve for SLC31A1. The AUC is 0.972, with 95%CI of 0.895-1.000, indicating excellent diagnostic performance. D: ROC curve for VEGFA. The AUC is 0.806, with 95%CI of 0.558-1.000, indicating good diagnostic performance. [a]*P*<0.05; [b]*P*<0.01. GEO: Gene expression omnibus; AMD: Age-related macular degeneration; ROC: Receiver operating characteristic; AUC: Area under the curve; TPR: True positive rate; FPR: False positive rate.

molecular and immune infiltration status of AMD patients.

In recent years, machine learning models have been widely used for AMD research, including risk factors analysis, image processing, disease diagnosis and therapeutic effect assessment[25-27]. In present study, we used three machine learning methods (Lasso, SVM, and Random Forest), as well as an ensemble of these models to predict the signature genes associated with AMD. By taking the intersection, we obtained six important variables (*ATP7A*, *DBT*, *VEGFA*, *UBE2D3*, *CP* and *SLC31A1*) as signature genes.

ATP7A is the main copper transporter for cellular copper export. Under normal copper level, *ATP7A* is located in the trans-Golgi network cavity predominantly and pumps copper from cytosol into the trans-Golgi network cavity. *ATP7A* translocated from the trans-Golgi network (TGN) to the plasma membrane and exports excess copper when there is an excess of copper. *ATP7A* is expressed in most tissues and organs, and

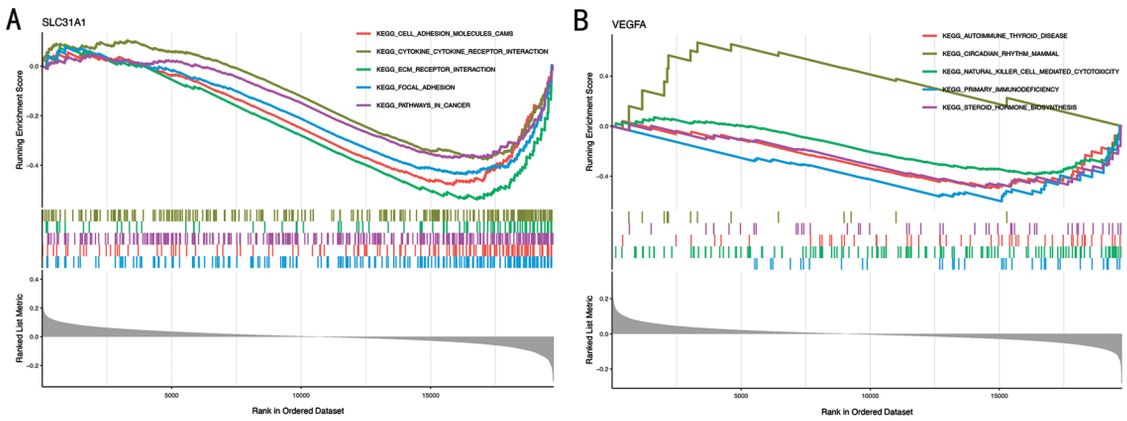

Figure 6 GSEA identifies the signaling pathways that are impacted by *SLC31A1* and *VEGFA* A: GSEA investigation of *SLC31A1*. The y-axis represents the pathways, the x-axis represents the rank in the ordered dataset. The plot shows the enrichment of *SLC31A1* in these pathways, indicating its potential role in cell adhesion, cytokine interaction, extracellular matrix-receptor interaction, and focal adhesion. B: GSEA investigation of *VEGFA*. The y-axis represents the pathways, the x-axis represents the rank in the ordered dataset. The plot shows the enrichment of *VEGFA* in these pathways, indicating its potential role in various biological processes related to angiogenesis and tissue remodeling. GSEA: Gene set enrichment analysis.

the mutation of *ATP7A* gene will lead to the genetic disorder of copper metabolism, resulting in Menkes disease[24]. *ATP7A* is also involved in a variety of tumorigenic mechanisms, promoting tumor cell invasion by providing sufficient copper ions to carcinogenic enzymes, such as colorectal cancer[28], hepatocellular carcinoma[29], and ovarian cancer[30]. *DBT* is a component of the branched-chain α-keto acid dehydrogenase complex, and its deficiency allows the accumulation of branched-chain amino acids and their harmful derivatives in the body[31]. *VEGFA* is one of the vascular endothelial growth factor (VEGF) family members that is most closely associated with neovascularization. VEGF is secreted mainly by retina glial cells, retinal ganglion cells, cells in the inner nuclear layer, RPE cells and pericytes in the eye. Under ischemia and hypoxia conditions, retina glial cells, RPE cells and vascular endothelial cells are activated. Anti-VEGF treatments were currently the main therapy for nAMD, including small molecule (pegaptanib) and antibody (aflibercept)[32-33]. UBE2D3 (also known as UBCH5C) is a ubiquitin crosslinking enzyme that regulates basic cell activities, including apoptosis, DNA damage response, ischemia reperfusion, tumorigenesis and cell cycle control, by participating in the ubiquitin proteasome pathway[34]. Ceruloplasmin (CP) is transported through bile after synthesis in liver and taken up by other tissues and organs to play such roles as oxidation and antioxidant, participate in iron transportation, regulate copper transport and metabolism. Lack of CP will cause damage to kidney, blood system, skin, skeletal muscle, endocrine and other organs[35-36]. In ATP7A-related disease, low ceruloplasmin is a more sensitive and discriminative biomarker than serum copper[37]. Previous studies have found that mice with targeted mutation of CP and its cognate Hephaestion showed age-related retinal iron accumulation and retinal degeneration with characteristics which was similar to human AMD[38]. In validation of the external dataset, it was found that, SLC31A1 and VEGFA had the best predictive accuracy as the AUC were 0.972 and 0.806, respectively. The difference in expression between CNV group and control group of the two genes were also confirmed by *in vitro* assays. Accordingly, SLC31A1 and VEGFA was selected as biomarkers for further analysis. There was a lot of current research surrounding the role of VEGFA in AMD but reports about SLC31A1 and AMD are very few.

SLC31A1 (also known as copper transporter 1, CTR1), the primary copper ion transporter, mediates the uptake of copper ions (Cu^{+}) into cells, thereby maintaining intracellular copper homeostasis. Its activity can be modulated under conditions of copper excess or deficiency to restore copper homeostasis[3]. In AMD, altered expression or function of SLC31A1 may disrupt intracellular copper levels in RPE cells, inducing copper-dependent cell death and subsequent cell death[7]. Copper ions can induce the formation of S-nitrosylated proteins, key mediators of copper-dependent cell death. Copper uptake mediated by SLC31A1 may influence the levels of S-nitrosylated proteins in RPE cells, thereby modulating the copper-dependent cell death pathway. This may significantly impact the survival and function of RPE cells in AMD. Furthermore, copper ions are known to regulate the functions of immune cells, including macrophages and T cells[39-40]. SLC31A1 may influence retinal immune responses by modulating copper availability in immune cells. For instance, copper can enhance the production of pro-inflammatory cytokines and promote macrophage activation. In AMD, SLC31A1 may promote a chronic inflammatory state by modulating copper homeostasis in immune cells,

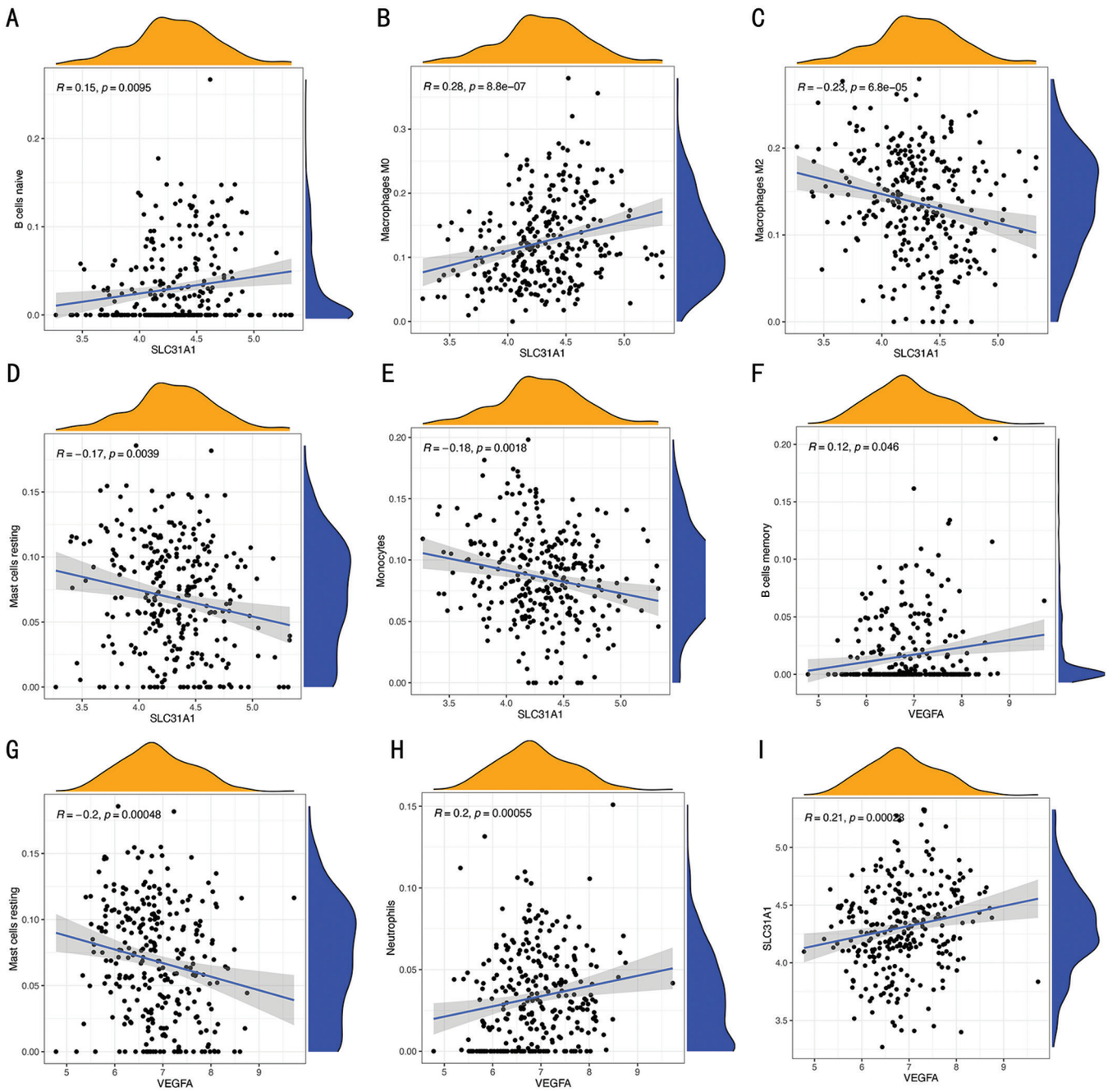

Figure 7 Correlation analysis between infiltrating immune cells and hub genes A-H: The scatter plot showing the correlation between hub gene (*SLC31A1* or *VEGFA*) and various infiltrating immune cells. The x-axis represents the hub gene, and the y-axis represents different infiltrating immune cells. A: *SLC31A1* and naïve B cells; B: *SLC31A1* and M0 macrophages; C: *SLC31A1* and M2 macrophages; D: *SLC31A1* and resting mast cells; E: *SLC31A1* and monocytes; F: *VEGFA* and memory B cells; G: *VEGFA* and resting mast cells; H: *VEGFA* and neutrophils; I: The scatter plot showing the correlation between *SLC31A1* and *VEGFA*.

thereby further impacting disease progression. Therefore, the role of SLC31A1 in copper-dependent cell death and immune interactions may make it a potential candidate for AMD biomarkers and therapeutic targets.

This study has some limitations. First, the number of data sets studied in this study is relatively limited. Additional multicenter external data sets are needed to confirm the specific molecular mechanisms of biomarkers in the pathogenesis of AMD. Second, the laser-induced CNV model primarily mimics neovascular AMD but does not fully recapitulate the chronic immune dysregulation or geographic atrophy seen in human AMD. Efforts are ongoing to collect human specimens for further investigations.

In-depth study of the specific function and action pathway of immune molecules in the occurrence and development of AMD is helpful to find a new method of immunotherapy for AMD. Our results identified two characteristic cuprotosis-related genes *SLC31A1* and *VEGFA* involved in the immune process of AMD. *VEGF* targeting therapy is currently the mainstream treatment for AMD, and correlation results in

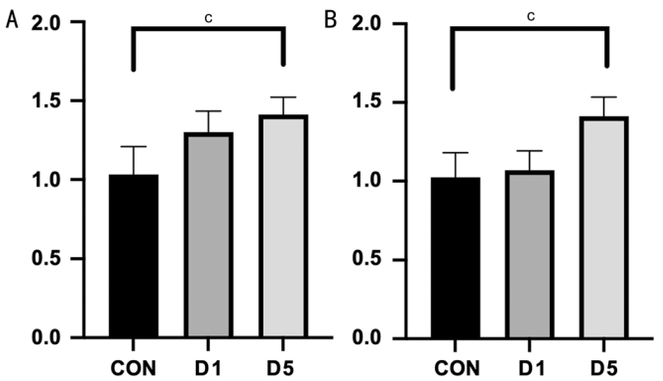

Figure 8 RT-PCR analysis of SLC31A1 and VEGFA expression levels A: The mRNA expression levels of SLC31A1 in the control group (CON) and laser-induced CNV model groups at day 1 (D1) and day 5 (D5). The y-axis represents the expression levels, and the x-axis represents the different groups (CON, D1, D5). B: The mRNA expression levels of VEGFA in the control group and laser-induced CNV model groups at D1 and D5. The y-axis represents the expression levels, and the x-axis represents the different groups. $^{c}P<0.001$. CNV: Choroidal neovascularization; RT-PCR: Reverse transcription polymerase chain reaction; VEGFA: Vascular endothelial growth factor A.

our study showed a significant positive correlation between *SLC31A1* and *VEGFA* expression. Therefore, it is reasonable to believe that *SLC31A1* could also be a new therapeutic target for AMD treatment. By modulating its activity, the copper balance in RPE cells may be restored, thereby reducing oxidative stress and inflammation. *SLC31A1* levels can be used to monitor the response to AMD treatment, reflecting the effectiveness of interventions targeting copper homeostasis or related pathways. Future research should validate its role as a biomarker and therapeutic target in larger, more diverse cohorts and explore specific *SLC31A1* modulators.

In conclusion, this study establishes a link between cuproptosis and AMD, identifying six key genes (*ATP7A*, *DBT*, *VEGFA*, *UBE2D3*, *CP*, *SLC31A1*) through machine learning. *SLC31A1* and *VEGFA* emerged as critical regulators of immune responses in AMD, validated in external datasets and a CNV mouse model. Our findings implicate cuproptosis in AMD pathogenesis, offering new diagnostic biomarkers and potential therapeutic targets for modulating copper-dependent pathways.

ACKNOWLEDGEMENTS

Conflicts of Interest: Li C, None; **Lu YC,** None; **Chen MX,** None.

REFERENCES

1 Mitchell P, Liew G, Gopinath B, *et al*. Age-related macular degeneration. *Lancet* 2018;392(10153):1147-1159.

2 Wallsh JO, Gallemore RP. Anti-VEGF-resistant retinal diseases: a review of the latest treatment options. *Cells* 2021;10(5):1049.

3 Tsvetkov P, Coy S, Petrova B, *et al*. Copper induces cell death by targeting lipoylated TCA cycle proteins. *Science* 2022;375(6586): 1254-1261.

4 Hu Q, Zhang X, Huang JY, *et al*. The STAT1-SLC31A1 axis: potential regulation of cuproptosis in diabetic retinopathy. *Gene* 2024;930:148861.

5 Ferrington DA, Fisher CR, Kowluru RA. Mitochondrial defects drive degenerative retinal diseases. *Trends Mol Med* 2020;26(1):105-118.

6 Erie JC, Good JA, Butz JA, *et al*. Reduced zinc and copper in the retinal pigment epithelium and choroid in age-related macular degeneration. *Am J Ophthalmol* 2009;147(2):276-282.e1.

7 Aloysius Dhivya M, Aberami S, Nikhalashree S, *et al*. Copper mediates mitochondrial biogenesis in retinal pigment epithelial cells. *Biochim Biophys Acta Mol Basis Dis* 2020;1866(10):165843.

8 Agrón E, Mares J, Clemons TE, *et al*. Dietary nutrient intake and progression to late age-related macular degeneration in the age-related eye disease studies 1 and 2. *Ophthalmology* 2021;128(3):425-442.

9 Han GG, Wei PH, He MQ, *et al*. Glucose metabolic characterization of human aqueous humor in relation to wet age-related macular degeneration. *Invest Ophthalmol Vis Sci* 2020;61(3):49.

10 Newman AM, Gallo NB, Hancox LS, *et al*. Systems-level analysis of age-related macular degeneration reveals global biomarkers and phenotype-specific functional networks. *Genome Med* 2012;4(2):16.

11 Schlecht A, Zhang PP, Wolf J, *et al*. Secreted phosphoprotein 1 expression in retinal mononuclear phagocytes links murine to human choroidal neovascularization. *Front Cell Dev Biol* 2020;8:618598.

12 Ritchie ME, Phipson B, Wu D, *et al*. Limma powers differential expression analyses for RNA-sequencing and microarray studies. *Nucleic Acids Res* 2015;43(7):e47.

13 Liu H. Pan-cancer profiles of the cuproptosis gene set. *Am J Cancer Res* 2022;12(8):4074-4081.

14 Li LR, Li L, Sun Q. High expression of cuproptosis-related SLC31A1 gene in relation to unfavorable outcome and deregulated immune cell infiltration in breast cancer: an analysis based on public databases. *BMC Bioinformatics* 2022;23(1):350.

15 Zhang GH, Sun JP, Zhang XW. A novel Cuproptosis-related LncRNA signature to predict prognosis in hepatocellular carcinoma. *Sci Rep* 2022;12(1):11325.

16 Huang Y, Yin DZ, Wu LN. Identification of cuproptosis-related subtypes and development of a prognostic signature in colorectal cancer. *Sci Rep* 2022;12(1):17348.

17 Newman AM, Liu CL, Green MR, *et al*. Robust enumeration of cell subsets from tissue expression profiles. *Nat Methods* 2015;12(5):453-457.

18 Tibshirani R. Regression shrinkage and selection *via* the lasso: a retrospective. *Journal of the Royal Statistical Society Series B: Statistical Methodology* 2011;73(3):273-282.

19 Noble WS. What is a support vector machine? *Nat Biotechnol* 2006;24(12):1565-1567.

20 Breiman L. Random forests. *Mach Learn* 2001;45(1):5-32.

21 Wu TZ, Hu EQ, Xu SB, *et al*. clusterProfiler 4.0: a universal enrichment tool for interpreting omics data. *Innovation* (*Camb*) 2021;2(3):100141.

22 Tang LX, Wang T, Li W, *et al*. Construction of cuproptosis-related lncRNAs/mRNAs model and prognostic prediction of hepatocellular carcinoma. *Am J Cancer Res* 2022;12(10):4693-4707.

23 Tang XH, Guo T, Wu XL, *et al*. Clinical significance and immune infiltration analyses of the cuproptosis-related human copper proteome in gastric cancer. *Biomolecules* 2022;12(10):1459.

24 Chen LY, Min JX, Wang FD. Copper homeostasis and cuproptosis in health and disease. *Signal Transduct Target Ther* 2022;7:378.

25 Vyas A, Raman S, Surya J, *et al*. The need for artificial intelligence based risk factor analysis for age-related macular degeneration: a review. *Diagnostics* (*Basel*) 2022;13(1):130.

26 Kalra G, Cetin H, Whitney J, *et al*. Machine learning-based automated detection and quantification of geographic atrophy and hypertransmission defects using spectral domain optical coherence tomography. *J Pers Med* 2022;13(1):37.

27 Arslan J, Benke KK. Application of machine learning to ranking predictors of anti-VEGF response. *Life* (*Basel*) 2022;12(11):1926.

28 Gao W, Huang Z, Duan JF, *et al*. Elesclomol induces copper-dependent ferroptosis in colorectal cancer cells *via* degradation of ATP7A. *Mol Oncol* 2021;15(12):3527-3544.

29 Shao K, Shen H, Chen XF, *et al*. Copper transporter gene ATP7A: a predictive biomarker for immunotherapy and targeted therapy in hepatocellular carcinoma. *Int Immunopharmacol* 2023;114:109518.

30 Fu LH, Zhang D, Yi N, *et al*. Circular RNA circPBX3 promotes cisplatin resistance of ovarian cancer cells *via* interacting with IGF_2BP_2 to stabilize ATP7A mRNA expression. *Hum Cell* 2022;35(5):1560-1576.

31 Podebrad F, Heil M, Reichert S, *et al*. 4, 5-dimethyl-3-hydroxy-2 [5H]-furanone (sotolone)—the odour of maple syrup urine disease. *J Inher Metab Disea* 1999;22(2):107-114.

32 Tolentino M. Systemic and ocular safety of intravitreal anti-VEGF therapies for ocular neovascular disease. *Surv Ophthalmol* 2011;56(2):95-113.

33 Chalam KV, Brar VS, Murthy RK. Human ciliary epithelium as a source of synthesis and secretion of vascular endothelial growth factor in neovascular glaucoma. *JAMA Ophthalmol* 2014;132(11):1350-1354.

34 Shi YH, Yuan BF, Zhu WT, *et al*. Ube2D3 and Ube2N are essential for RIG-I-mediated MAVS aggregation in antiviral innate immunity. *Nat Commun* 2017;8:15138.

35 Linder MC. Ceruloplasmin and other copper binding components of blood plasma and their functions: an update. *Metallomics* 2016;8(9):887-905.

36 Liu ZD, Wang M, Zhang CB, *et al*. Molecular functions of ceruloplasmin in metabolic disease pathology. *Diabetes Metab Syndr Obes* 2022;15:695-711.

37 De Feyter S, Beyens A, Callewaert B. ATP7A-related copper transport disorders: a systematic review and definition of the clinical subtypes. *J Inherit Metab Dis* 2023;46(2):163-173.

38 Song DL, Dunaief JL. Retinal iron homeostasis in health and disease. *Front Aging Neurosci* 2013;5:24.

39 Karunadharma PP, Kapphahn RJ, Stahl MR, *et al*. Dissecting regulators of aging and age-related macular degeneration in the retinal pigment epithelium. *Oxid Med Cell Longev* 2022;2022:6009787.

40 Wong JHC, Ma JYW, Jobling AI, *et al*. Exploring the pathogenesis of age-related macular degeneration: a review of the interplay between retinal pigment epithelium dysfunction and the innate immune system. *Front Neurosci* 2022;16:1009599.